Predicting the medium-temperature thermal stability of impact-strengthened medium-thick plate aluminum alloy using a back propagation artificial neural network

Xiuliang Wang [a], Yibo Ai [a], Weidong Zhang [a,*], Shuai Ji [b,**], Haili Wang [b]

[a] National Center for Materials Service Safety, University of Science and Technology Beijing, Beijing, 10083, China
[b] School of Materials Science and Engineering, Xi'an Shiyou University, 710065, China

ABSTRACT

A normalized medium-thick plate of aluminum alloy (4038) was impact-strengthened using a free-fall method at room temperature (approximately 20 °C). Specimens were then aged at 450 °C, 550 °C and 650 °C for 10, 20, 30 and 40 min respectively. Micro-hardness of each sample was tested. Micro-structure of samples annealed at 650 °C for different durations was characterized. A three-layer back propagation artificial neural network (BPANN) was trained using actual state parameters of the prepared samples. Results reveal that medium-temperature thermal stability of the prepared plate can be predicted through the BPANN model. Deviation of predicted values from the experimental ones is within 6 %, with a prediction accuracy exceeding 94 %. Variation trend of the predicted and the experimental thermal stability is consistent, but the predicted values are all higher than the measurements. Prediction accuracy of BPANN can be improved by increasing convergence rate of the error function. By adding relevant parameters of the micro-structure from samples aged at 650 °C to the input layer, BPANN model further improve its output and approach the real state of samples. The findings of this study can help researchers reduce the number and cost of experiments. The aim of this work was to predict the medium-temperature thermal stability of impact-strengthened normalized medium-thick plate of aluminum alloy annealed at different temperatures, and it also can be used as reference for other similar experiments.

Artificial neural networks (ANNs) are bionic structure and function information processing systems. ANNs are a network composed of interconnected artificial neurons that function as nodes. They are abstracted models simulating the micro-structure and function of the human brain. Hence, they can emulate certain fundamental features of the human brain and represent a crucial approach for simulating human intelligence [1–4]. Therefore, ANNs exhibit outstanding attributes such as self-learning, self-organization, self-adaptation, rapid processing, high fault tolerance, memory association, and an ability to approximate arbitrary complex nonlinear systems. These networks are trained on numerous experimentally measured values, after which they can summarize the variations in experimental data through a finite number of overlapping calculations without requiring a formula in advance.

ANNs have also been used for predicting various properties of alloy materials. Extensive research in the field of material science and

---

engineering has revealed that material properties follow the characteristics of nonlinear systems. The properties of alloys, such as thermal stability, strength and ductility, are complex functions of various factors, including micro-structure, temperature and pressure etc. Then ANNs are suitable for providing strategies and predictions to address a multitude of challenges regarding material performance, such as predicting phase transformations and estimating deficiencies in materials. Recently, several ANN and back propagation network models have been developed for predicting the performance of metal materials [5–9].

A back propagation network is a multi-layer feed forward network composed of numerous linear and nonlinear processing units. Its activation function is continuously differentiable, enabling its accurate calculation via the gradient method. Moreover, the process of learning the analytical formula of weight can be well defined. Therefore, the back propagation network realize the nonlinear mapping of arbitrary inputs to outputs as per the real-world working conditions [10–14].

Aluminum alloys are commonly used in medium-thick plates, which are widely employed in aerospace, machinery manufacturing, land transportation, and national defense industry owing to their outstanding performance [15–18]. Fatigue is a prominent contributor to the failure of these aluminum plates, which typically begins on surface of the alloys in service [19–21]. The service capacity of metal materials can be improved by adopting simple procedures to improve the failure resistance of the surface [22–24]. To improve the fatigue resistance of aluminum plates in engineering application under medium and high temperature conditions [25–28], the high surface hardness, wear resistance, toughness and plasticity of the alloy is required.

Impact of aluminum components at room temperature refines the grains in the alloy and improve the hardness, strength, and wear resistance, thereby enhancing the overall mechanical properties. Given the increasing demands for medium to high-temperature working conditions in engineering, the medium-temperature thermal stability of normalized aluminum medium-thick plate after impact strengthening has become a critical criterion for material selection [29–32].

In this study, we focused on the medium-temperature thermal stability of normalized aluminum medium-thick plates after impact strengthening. To predict the thermal stability of the alloy, a back propagation artificial neural network (BPANN) model was trained.

1. Materials and experimental procedures

An aluminum (4038) medium-thick plate bar (diameter: 8 mm) produced in China was used as the raw material. Table 1 lists its elemental compositions (mass fraction of alloying elements, wt.%). The aluminum medium-thick plate bar was cut into cylindrical samples, as shown in Fig. 1. The samples were normalized, by annealing at 450 °C for 15 min, and then cooling in air to room temperature. After normalizing, the samples were subjected to impact strengthening. An iron body with 18 kg was dropped freely from a predefined height of 2.2 m, impacting the samples, as shown in Fig. 2. The preparing conditions of samples in this work are listed in Table 2.

A micro-hardness tester (HVS-1000Z) was used to measure the micro-hardness of samples (load: 2 kg and load time: 10 s). The hardness was tested from the center to the edge of each sample, with the separating distance of 1 mm between adjacent points. The micro-structure along the radius of samples is not uniform after impact strengthening.

2. BPANN algorithm and implementation

In the back propagation algorithm, the signal input propagates forward in the network, while the error signal (the difference between the desired and actual outputs) propagates backward. The sigmoid input–output relation was used to represent the nonlinear neurons comprising the back propagation network used in this study, as shown below.

$$f(w_i) = 1 / (1 + e^{-w_i}) = 1 / \left(1 + e^{-\left(\sum m_j n_j - \theta_i\right)}\right) \tag{2–1}$$

where, $f(w_i)$ is the output of each layer, $w_i = \sum m_j n_j - \theta_i$ is the input of node i in the current layer. The first derivative of $f(w_i)$ exists and satisfies the condition that the input and the output are nonlinear and monotonically rising.

The back propagation algorithm uses delta learning law and gradient search to minimize the mean square deviation between the expected output and actual outputs. A three-layer BPANN is consisted of input, middle, and output layers containing a, b and c number of neurons, respectively, and the connection weights between front and back adjacent layers are w_{ab} and w_{bc}, and the threshold is G. The network is trained by collecting P learning samples from experimental data, namely $x_1, x_2 ..., x_P$. The corresponding expected outputs are $y_1, y_2 ... y_P$. The actual outputs are $z_1, z_2 ... z_P$. For a sample set, P_1 (h = 1, 2 ..., g), the error at the output layer is as following:

$$E_{P_1} = \frac{1}{2} \sum_{h=1}^{g} (yh - z_h)^2 \tag{2-2}$$

The inclusion of 1/2 in the above formula is because of the sample's cylindrical shape, which is symmetrical about the center of the

Table 1

Chemical composition of aluminum alloy (4038) medium-thick plate (wt%) .

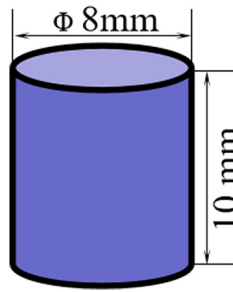| element	Mg	Ni	Cr	C	P	S	Si	Al
content	0.086	0.026	0.012	0.083	0.008	0.011	0.032	balance

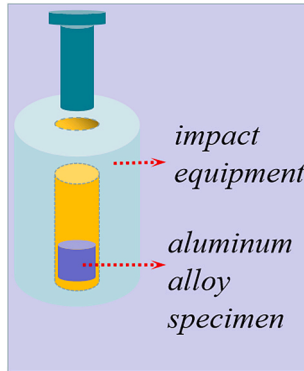**Fig. 1.** Aluminum alloy medium-thick plate sample.

Fig. 2. Impact strengthening device.

Table 2
Aging treatment of samples in two states.

Medium- temperature aging treatment	Different states of two aluminum medium plate samples	
	Normalized aluminum medium-thick plate	Normalized aluminum medium-thick plate after impact strengthening
Holding time/min	10 20 30 40	10 20 30 40
Heating temperature/°C	450, 550, 650	450, 550, 650
Cooling	Air cooling to room temperature	Air cooling to room temperature

end face. The micro-hardness values were obtained point by point, starting from the center to the edge of the samples on the end face. In view of the symmetrical structure of the samples, the points at the same radius are equivalent. Then the average hardness at equivalent points were used. This is reflected in equations (2) and (3).

The total error for P number of samples is:

$$E_P = \frac{1}{2} \sum_{P=1}^{P} \left[\sum_{h=1}^{g} (y_h - z_h)^2 \right] \tag{2-3}$$

The gradient method is used to adjust each connection weight by equations (2)–(4), as shown below.

$$\nabla w_{ab} = -\sum_{P} \eta \left(\partial E_P / \partial w_{ab} \right) \tag{2-4}$$

Following formula (2-4),

$$\nabla w_{ab} = w_{ab(h+1)} - w_{ab(h)} = -\sum_{P} \eta \left(\partial E_P / \partial w_{ab} \right) = \sum_{P} \eta \left(\partial \left(\frac{1}{2} \sum_{P=1}^{P} \left[\sum_{h=1}^{g} (y_h - z_h)^2 \right] \right) / \partial w_{ab} \right) = \eta \sum_{P} \delta_{ab} \cdot x_{ab}$$

The weights of the three-layer BPANN are given by equations (2)–(5), as shown below.

$$w_{ab}(h+1) = w_{ab}(h) + \eta \sum_P \delta_{ab} \cdot x_{ab} \tag{2–5}$$

The above approach used for weight correction which is also known as batch processing, is implemented by calculating the total error after all samples are entered. This correction process ensures that the total error tends to decrease as the learning progresses. When multiple copies are available, the batch processing converges rapidly.

The entire learning process of the BPANN consists of two parts. The first part is the calculation of the input signal from the bottom up, i.e., from the neurons in the output layer. The second part is the computation of the error signal from the top down, i.e., from the modification of the weights or thresholds. The two stages are converged by alternating repeatedly.

The BP algorithm is implemented as following, and the corresponding flowchart is shown in Fig. 3.

(1) Initialize the network. The weights and thresholds are evenly distributed in the range of [0,1].
(2) Successively input the learning samples (P) into the network, then calculate the output of each layer.
(3) Calculate errors at the output layer.
(4) Compute the total error after all the learning samples in P are entered into the network. Then, determine whether the error meets the required standard. If it does, halt the process; otherwise, enter the next step.
(5) Back propagate the error to each output layer by layer and adjust the corresponding weights and threshold. Return to step (2) until the error reduced under standard.

3. Prediction of the thermal stability using BPANN

Since the micro-hardness of the aluminum alloy changes with the conditions of heat treatment, here the micro-hardness is used as an indicator for the thermal stability under medium temperature. Then the micro-hardness is entered into the BPANN model as an equivalent of the thermal stability in the present work. The thermal stability data obtained at 450 °C and 550 °C for different holding times were used to train the network, then the thermal stability at 650 °C for different holding times was predicted using the trained model.

In this study, a BPANN model with three layers was adopted, and the number of input-layer units was determined based on factors that significantly influence the medium-temperature thermal stability of the impact-strengthened aluminum medium-thick plate. The BPANN structure adopted in this study is shown in Fig. 4 There are six factors in the input layer, which are the annealing temperature and duration, the sample size, the micro-structure, the testing location, and the cooling rate. The middle layer consists of eleven nodes. The output layer provides the micro-hardness. The micro-hardness used for model training is listed in Tables 3 and 4Fig. 5).

Based on the BPANN model, prediction of the thermal stability is implemented as following. Firstly, micro-hardness of the samples annealed at 450 °C was used to train the ANN model until the error function converged. Secondly, using the trained model after the first step, micro-hardness of the samples annealed at 550 °C for different durations was predicted. The predicted result at 550 °C is
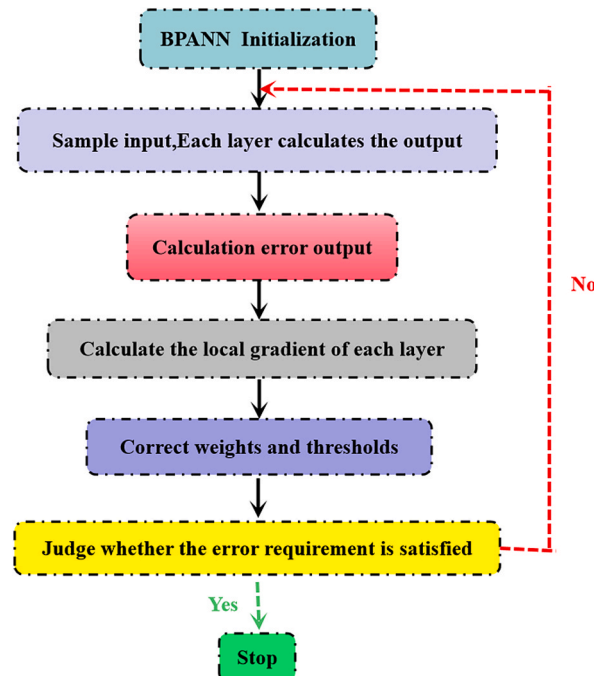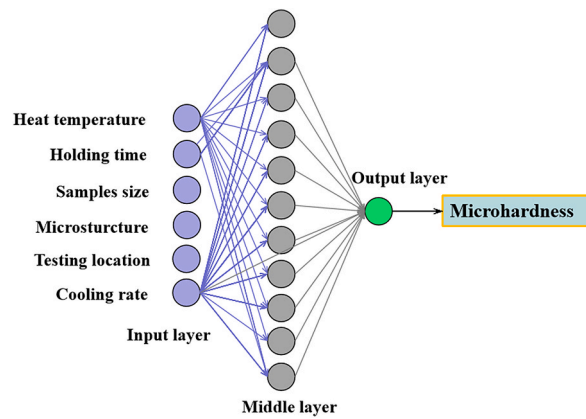

Fig. 3. BPANN program flow.
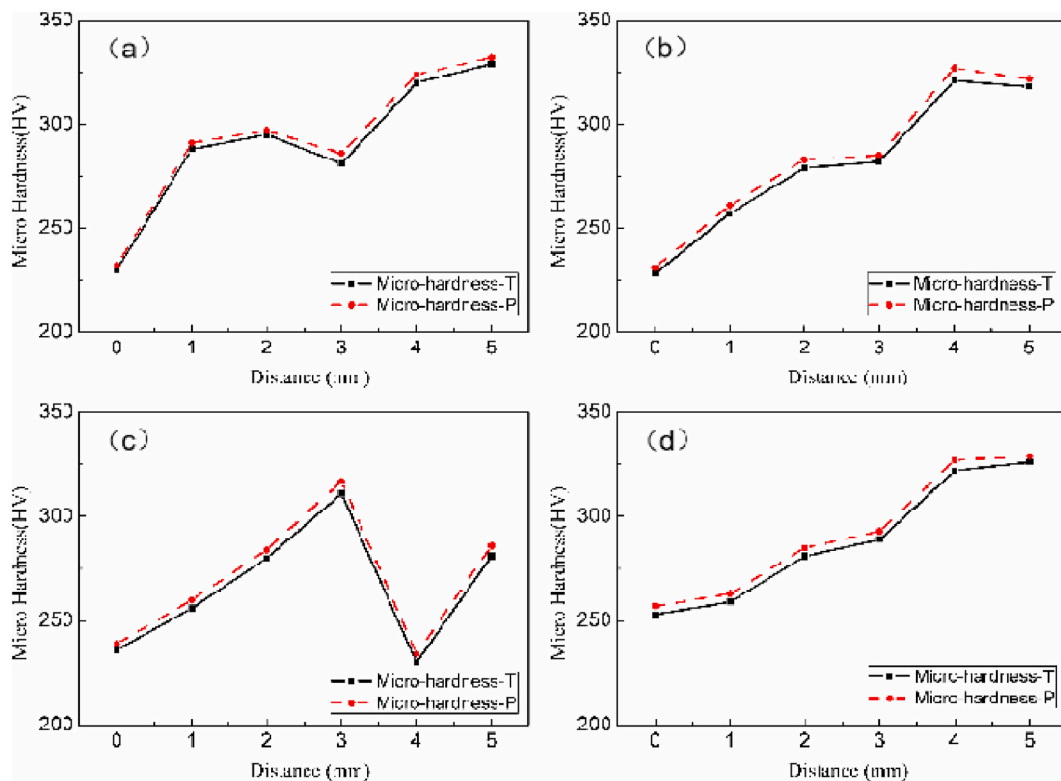
Fig. 4. BPANN structure.

Fig. 5. Measured and predicted micro-hardness of normalized aluminum alloy medium-thick plate after impact strengthening at 450 °C for a holding time of (a) 10 min, (b) 20 min, (c) 30 min, and (d) 40 min.

presented in Table 5. By comparing the predicted and the measured values, the prediction accuracy as well as the output error was estimated. Thirdly, the adjusted error function was back-propagated into the network, and the measured micro-hardness values of samples annealed at 450 °C and 550 °C were used to train the network again. Fourthly, the micro-hardness of samples annealed at 650 °C was predicted, and the errors are estimated as step 2. The predictions and the experimental measures at 650 °C are listed in Tables 6 and 7 respectively.

When only the data at 450 °C is used for model training, the predicted micro-hardness deviates from the corresponding measured value by 9–14 % as shown by the difference between Tables 4 and 5, due to the insufficient number of training samples, which reduces the gradient and convergence rate of the error function. However, it is noted that all the predictions are higher than the test values. The BPANN model demonstrates a stable forecasting behavior.

Further adding the data at 550 °C to train the BPANN model, the deviation from the predictions to the measures reduces to below 6
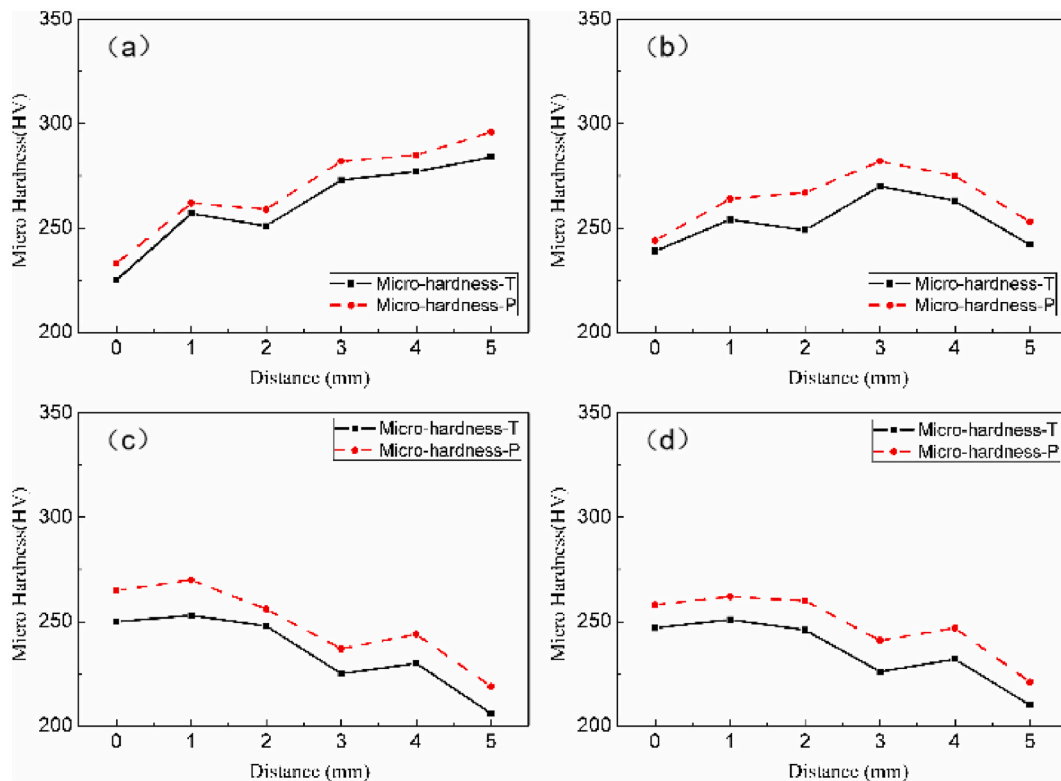
Fig. 6. Measured and predicted micro-hardness of normalized aluminum alloy medium-thick plate after impact strengthening at 550 °C for a holding time of (a) 10 min, (b) 20 min, (c) 30 min, and (d) 40 min.

Table 3
Micro-hardness of impact-strengthened normalized aluminum alloy medium-thick plate at 450 °C for different holding times.

Heat temperature/°C		450			
Holding time/min		10	20	30	40
Micro-hardness/HV	Samples center	230	228	236	253
	1 mm from the center	288	257	256	259
	2 mm from the center	295	279	280	281
	3 mm from the center	281	282	311	289
	4 mm from the center	320	321	230	322
	5 mm from the center	329	318	281	326

Table 4
Micro-hardness of impact-strengthened normalized aluminum alloy medium-thick plate at 550 °C for different holding times.

Heat temperature/°C		550			
Holding time/min		10	20	30	40
Micro-hardness/HV	Samples center	225	239	250	247
	1 mm from the center	257	254	253	251
	2 mm from the center	251	249	248	246
	3 mm from the center	273	270	225	226
	4 mm from the center	277	263	230	232
	5 mm from the center	284	242	206	210

%, with a prediction accuracy exceeding 94 %, indicating a significant improvement in precision of the artificial neuron network. A comparison of Tables 6 and 7 shows that the predictions consistently surpass the observed values.

To verify the positive deviation of the prediction from the experimental value, the data from samples annealed at 550 °C and 650 °C were used to train the BPANN model, and the thermal stability at 450 °C was predicted using the trained network, and the difference between the predictions and the test values was examined. Accuracy of the trained network and the convergence condition of the error

Table 5
Predicted micro-hardness of impact-strengthened normalized aluminum alloy medium-thick plate heat-treated at 550 °C for different holding times.

Heat temperature/°C		550			
Holding time/min		10	20	30	40
Micro-hardness/HV	Samples center	233	244	265	258
	1 mm from the center	262	264	270	262
	2 mm from the center	259	267	256	260
	3 mm from the center	282	282	237	241
	4 mm from the center	285	275	244	247
	5 mm from the center	296	253	219	221

Table 6
Predicted micro-hardness of impact-strengthened normalized aluminum alloy medium-thick plate heat-treated at 650 °C for different holding times.

Heat temperature/°C		650			
Holding time/min		10	20	30	40
Micro-hardness/HV	Samples center	255	209	194	175
	1 mm from the center	198	197	200	180
	2 mm from the center	246	185	184	171
	3 mm from the center	217	172	173	173
	4 mm from the center	191	193	185	161
	5 mm from the center	203	183	184	182

Table 7
Micro-hardness of impact-strengthened normalized aluminum alloy medium-thick plate at 650 °C for different holding times.

Heat temperature/°C		650			
Holding time/min		10	20	30	40
Micro-hardness/HV	Samples center	252	197	182	163
	1 mm from the center	193	189	187	169
	2 mm from the center	239	173	170	157
	3 mm from the center	208	161	160	160
	4 mm from the center	183	182	174	149
	5 mm from the center	194	171	172	170

function were also evaluated via several experimental procedures. Predictions of the thermal stability at 450 °C are presented in Table 8. The difference between Tables 8 and 3 still shows that the predictions are slightly higher than the measured results.

The errors of predictions are irrelevant with the annealing temperature. Specifically, among the three annealing temperatures shown in Figs. 5–7, i.e., 450 °C, 550 °C and 650 °C, the error at 550 °C is the largest, and the error at 450 °C is the smallest, with the error at 650 °C being in the middle. Close examination of the data shows that the deviation of the predictions from the measurements decreases with the increasing number of training datasets. At 550 °C, 650 °C and 450 °C, the number of training datasets used for predictions increases, and the error of predictions decreases.

Internal micro-structure of the samples varies significantly with positions after the impact strengthening, leading to the uneven distribution of micro-hardness from center to edge of the samples. The proposed BPANN model predicts such changes in the medium-thick plate of aluminum alloys accurately. Such ability of BPANN model is useful for estimating the strength of the alloys, which is important for engineers to control mechanical properties of the aluminum components and reduce the experimental cost.

Micro-structure of the impacted samples after annealing at 650 °C is shown in Fig. 8Fig. 7. With increasing of the annealing duration from 10 min to 40 min, the micro-structure recovers gradually as shown in Fig. 8 (a)–(d). The recovering of micro-structure results in the reduction of hardness with annealing time.
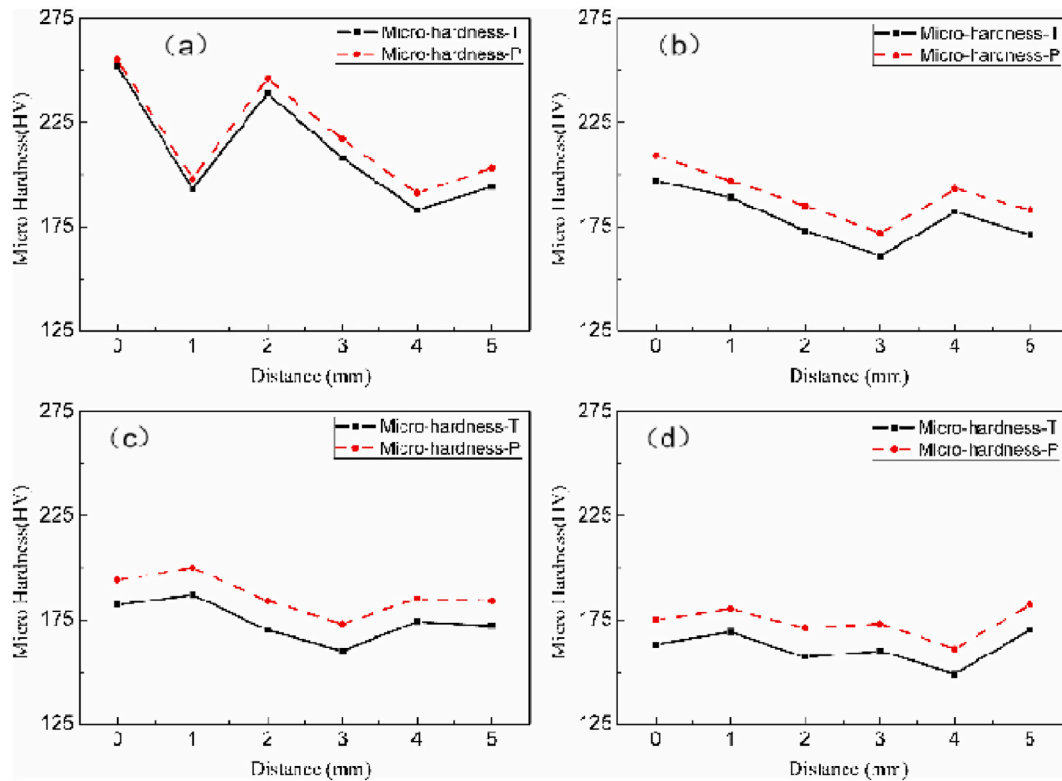
During the process of impact strengthening, the aluminum substrate deforms plastically rapidly by absorbing the impact energy, and the temperature in the sample also rise instantly, resulting in the refinement of the grains and the dissolution of secondary phases. During annealing these phases precipitate again as shown in Fig. 8 (a), leading to the secondary hardening phenomenon. The hardness of samples with precipitated hard phase is listed in Table 7. Further increasing the annealing time leads to the coarsening of both the grains and the secondary phases as shown in Fig. 8 (b)–(d), meanwhile the hardness continuously decreases.

According to the principles in materials science, the mechanical properties of an alloy is determined by its micro-structure. For an artificial neuron network, it does not understand these principles, however, the more relevant parameters enter into the network, the more accurate predictions can the model give. Since the micro-structure is one of the key factors influencing the hardness of the alloy, the phase composition is also a crucial parameter for the BPANN model.

Table 8

Predicted micro-hardness of impact-strengthened normalized aluminum alloy medium-thick plate heat-treated at 450 °C for different holding times.

Heat temperature/°C		450			
Holding time/min		10	20	30	40
Micro-hardness/HV	Samples center	232	231	239	257
	1 mm from the center	291	261	260	263
	2 mm from the center	297	283	284	285
	3 mm from the center	286	285	317	293
	4 mm from the center	324	327	234	327
	5 mm from the center	332	322	286	329

Fig. 7. Measured and predicted micro-hardness of impact-strengthened normalized aluminum alloy medium-thick plate heat-treated at 650 °C for a holding time of (a) 10 min, (b) 20 min, (c) 30 min, (d) 40 min.

4. Conclusion

(1) The medium-thick aluminum plates were prepared by room temperature impact and aging. To predict the thermal stability of the aluminum plates, the BPANN model was trained with the main state parameters of the samples. By optimizing the training strategy, the trained BPANN model predicts thermal stability of the aluminum plates with an accuracy over 94 %, or with the error being controlled under 6 %.

(2) The predictions varies synchronously with the measurements at different locations. And the predictions are higher than the test values owing to the limited number of training samples. Prediction accuracy of the network can be improved by increasing convergence rate of the error function.

(3) Outputs of the BPANN model are consistent with the change of micro-structure in prepared samples, indicating that the key to improve accuracy of the model is to use more relevant parameters to train it.

Fund project
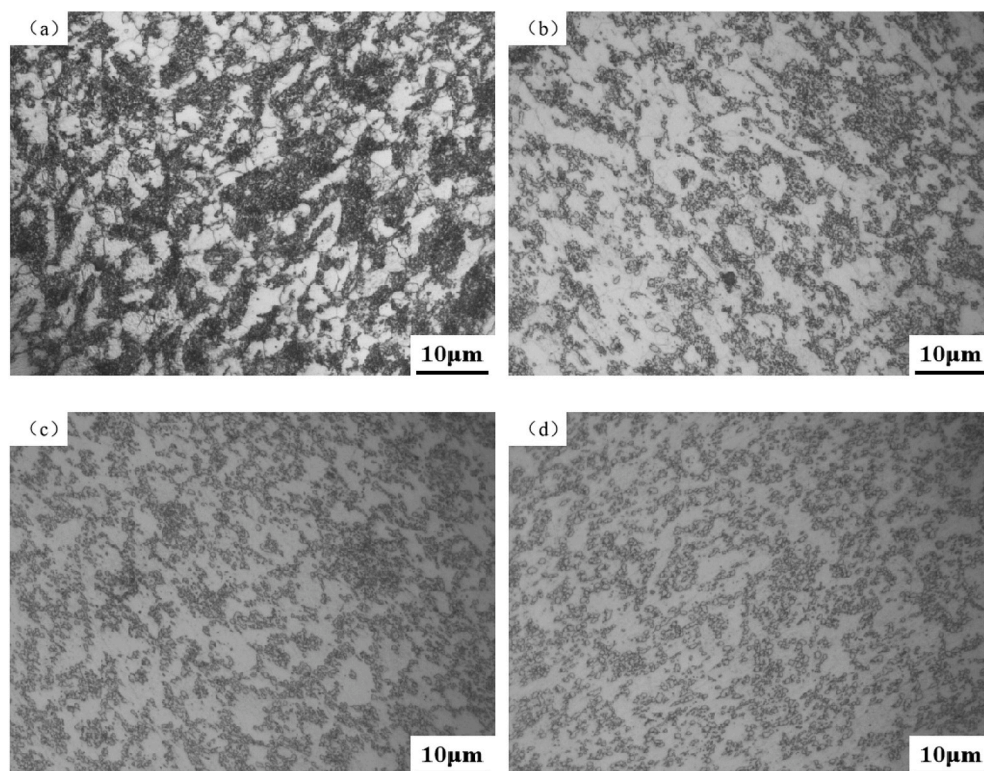
Fig. 8. Morphology of normalized aluminum alloy medium-thick plate after impact strengthening kept at 650 °C: (a) 10min; (b) 20min; (c) 30min; (d)40min.

CRediT authorship contribution statement

Xiuliang Wang: Validation, Software, Investigation. **Yibo Ai:** Supervision. **Weidong Zhang:** Writing – review & editing, Visualization, Project administration, Funding acquisition. **Shuai Ji:** Writing – original draft, Formal analysis. **Haili Wang:** Methodology.

Declaration of competing interest

The authors declare that they have no known competing financial interests or personal relationships that could have appeared to influence the work reported in this paper.

References

[1] Yanxia Liu, Xinchen Gao, The applications of BP neural networks in the material field, J. Liaoning Univ. (Nat. Sci. Ed.) 34 (2) (2007) 116–119.
[2] Xiaoling Liu, Shuncheng Song, Honggang Shi, Fujun Shang, Prediction of tungsten tensile strength with artificial BP neural network method, Mater. Sci. Technol. 34 (2) (2006) 116–119.
[3] Pin Zhou, Design and Application of MATLAB Neural network, Tsinghua University Press, Beijing, 2013.
[4] Yu Sun, Weidong Zeng, Yongqing Zhao, et al., Modeling of constitutive relationship of Ti600 alloy using BP artificial neural network, Rare Met. Mater. Eng. 40 (2) (2011) 220–224.
[5] Y. Pang, P. Lin, Q. Sun, et al., Experimental and numerical analyses of aluminum alloy medium-thick plate during three dimensional severe plastic deformation (3D-SPD), Arch. Civ. Mech. Eng. 20 (4) (2020) 104.
[6] Y. Chang, Z. Kuang, R. Tang, et al., Investigation of anisotropic subsequent yield behavior for aluminum alloy medium-thick plate by the distortional yield surface constitutive model, J. Mater. 13 (5) (2020) 1196.
[7] Y. Cao, Y.J. Zhang, T.Y. Yang, Effect of addition of montmorillonite and indium composite powder on tribological properties of aluminum alloy medium-thick plate friction pairs, Key Eng. Mater. (2020) 866.
[8] Z. Guo, W. Sha, Modelling the correlation between processing parameters and properties of maraging steels using artificial neural network, Comput. Mater. Sci. 29 (2004) 12–28.
[9] N.G. Dudkina, Development of inelastic deformation upon electrical mechanical treatment and surface plastic deformation of grade aluminum alloy medium-thick plate, J. Mach. Manuf. Reliab. 49 (2) (2020) 116–121.
[10] W. Hao, C. Ping, L. Yang, et al., Effect of axial vibration on sliding frictional force between shale and aluminum alloy medium-thick plate, Shock Vib. 2018 (PT.1) (2018) 1–13, 2018-1-24), 2018.
[11] S. Malinov, W. Sha, J.J. Mckeown, Modelling the correlation between processing and properties in titanium alloys using artificial neural network, Comput. Mater. Sci. 21 (2001) 375–394.
[12] Y. Sun, W.D. Zeng, Y.Q. Zhao, et al., Development of constitutive relationship model of Ti600 alloy using artificial neural network, Comput. Mater. Sci. 48 (2010) 686–691.

[13] P. Li, K.M. Xue, Y. Lu, J.R. Tan, Neural network prediction of flow stress of Ti-15-3 alloy under hot compression, J. Mater. Process. Technol. 148 (2004) 235–238.

[14] R. Kapoor, D. Pal, J.K. Chakravartty, Use of artificial neural networks to predict the deformation behavior of Zr–2.5Nb–0.5Cu, J. Mater. Process. Technol. 169 (2005) 199–205.

[15] C.H. Dong, Artificial Neural Network and Application with MATLAB, National Defense Industry Press, Beijing, 2005.

[16] M.T. Hagan, H.B. Demuth, M. Beale, Neural Network Design, Thomson Learning, Singapore, 2002.

[17] J.M. Zurada, Introduction to Artificial Neural Networks, West Publishing Co, New York, 1992.

[18] E. Omer, K. Erdogan, P. Murat, O. Erdogan, Prediction of martensite and austenite start temperatures of the Fe-based shape memory alloys by artificial neural networks, J. Mater. Process. Technol. 200 (2008) 146–152.

[19] P. Hao, A. He, W. Sun, Formation mechanism and control methods of inhomogeneous deformation during hot rough rolling of aluminum alloy plate, Arch. Civ. Mech. Eng. 18 (1) (2018) 245–255.

[20] G. Vincze, F.J. Simões, M.C. Butuc, Asymmetrical rolling of aluminum alloys and steels: a review, Metals 10 (9) (2020) 1126.

[21] S.H. Zhang, L. Deng, Q.Y. Zhang, Q.H. Li, J.X. Hou, Modeling of rolling force of ultra-heavy plate considering the influence of deformation penetration coefficient, Int. J. Mech. Sci. 159 (2019) 373–381.

[22] D. Pustovoytov, A. Pesin, P. Tandon, Asymmetric (hot, warm, cold, cryo) rolling of light alloys: a review, Metals 11 (6) (2021) 956.

[23] R. Branco, J.D. Costa, L.P. Borrego, S.C. Wu, X.Y. Long, F.C. Zhang, Effect of strain ratio on cyclic deformation behaviour of 7050-T6 aluminium alloy, Int. J. Fatig. 129 (2019) 1–12, 105234.

[24] Wojciech Macek, Dariusz Rozumek, Grzegorz M. Krolczyk, Surface topography analysis based on fatigue fractures obtained with bending of the 2017A-T4 alloy, J. Pre-proofs 1–19 (2019).

[25] Y. Wei, L. Gaosheng, C. Qingwu, Q345 ultra-heavy plate rolled with temperature gradient, Mater. Manuf. Process. 30 (1) (2015) 104–110.

[26] X. Chen, Q. Cai, B. Xie, Y. Yun, Z. Zhou, Simulation of micro-structure evolution in ultra-heavy plates rolling process based on abaqus secondary development, Steel Res. Int. 89 (12) (2018).

[27] X. Liu, X.H. Liu, M. Song, X.K. Sun, L.Z. Liu, Eoretical analysis of minimum metal foil thickness achievable by asymmetric rolling with fixed identical roll diameters, Trans. Nonferrous Metals Soc. China 26 (2) (2016) 501–507.

[28] X. Chen, Q. Cai, B. Xie, Y. Yun, Z. Zhou, Simulation of micro-structure evolution in ultra-heavy plates rolling process based on abaqus secondary development, Steel Res. Int. 89 (12) (2018).

[29] B.S. Xie, Q.W. Cai, X. Chen, A novel process for heavy plate: gradient temperature rolling, fast cooling, tempering, Mater. Sci. Technol. 35 (10) (2019) 1193–1203.

[30] S.H. Zhang, L.Z. Che, Modeling of rolling force of ultra heavy plate accounting for gradient temperature, Adv. Mech. Eng. 13 (9) (2021).

[31] P.J. Hao, J.N. Liu, Influence of snake rolling on metal flow in hot rolling of aluminum alloy thick plate, Mechanics Indust. 21 (5) (2020) 525.

[32] A.B. Richelsen, Numerical analysis of asymmetric rolling accounting for differences in friction, J. Mater. Process. Technol. 45 (1–4) (1994) 149–154.